Available online at BCREC website: https://bcrec.id

Bulletin of Chemical Reaction Engineering & Catalysis, 15 (3) 2020, 743-751

Research Article

Hydrocracking of *Calophyllum inophyllum* Oil Employing Co and/or Mo Supported on γ-Al_2O_3 for Biofuel Production

Wega Trisunaryanti*, T. Triyono, Muhammad Ali Ghoni, Dyah Ayu Fatmawati, Puspa Nindro Mahayuwati, Endah Suarsih

Department of Chemistry, Universitas Gadjah Mada, Yogyakarta, Indonesia

Received: 2nd August 2020; Revised: 28th September 2020; Accepted: 29th September 2020; Available online: 29th September 2020; Published regularly: December 2020

Abstract

Cobalt and/or Molybdenum based catalysts were simply dispersed on γ-Al_2O_3 through wet impregnation. The set of prepared monometallic and bimetallic catalysts of ${}_aCoO/\gamma$-Al_2O_3, ${}_aMoO/\gamma$-Al_2O_3, ${}_aCoO_aMoO/\gamma$-Al_2O_3, and ${}_bCoO_bMoO/\gamma$-Al_2O_3 were investigated and evaluated in the hydrocracking of *Calophyllum inophyllum* (CIO) which is not a food crop as well as rich in unsaturated fatty acid that potential to be converted into biofuel. Out of the prepared catalysts, ${}_aCoO_aMoO/\gamma$-Al_2O_3 with total metal content, acidity, and specific surface area of 13.62 wt%, 5.01 mmol.g^{-1}, and 107.67 $m^2.g^{-1}$, respectively, showed the best catalytic performance. The high metal loading of ${}_aCoO_aMoO/\gamma$-Al_2O_3 is favorable by producing 65.56 wt% liquid fraction through carbocation formation mechanism. It was selective to produce 8.61 wt% gasoline and 5.01 wt% diesel.

Keywords: Cobalt; Molybdenum; γ-Al_2O_3; hydrocracking; Calophyllum inophyllum

How to Cite: Trisunaryanti, W., Triyono, T., Ghoni, M.A., Fatmawati, D.A., Mahayuwati, P.N., Suarsih, E. (2020). Hydrocracking of Calophyllum inophyllum Oil Employing Co and/or Mo Supported on γ-Al_2O_3 for Biofuel Production. *Bulletin of Chemical Reaction Engineering & Catalysis*, 15(3), 743-751 (doi:10.9767/bcrec.15.3.8592.743-751)

Permalink/DOI: https://doi.org/10.9767/bcrec.15.3.8592.743-751

1. Introduction

The rapid depletion of fossil fuel as our primary energy resource has become a concern for many people, especially researchers since many years ago. As a limited resource, the continuous use of fossil fuel may cause completely used up. Moreover, fossil fuel grows environmental damage in producing carbon dioxide (CO_2) emissions [1] that contribute to global warming. At this stage, the search for alternative resources has been gaining much attention and currently under development in order to reduce dependence on fossil resources and suppressing global warming. One of the promising alternatives is biomass, which later is converted into biofuel. Biomass can be generated from many resources such as residues from agricultural, industrial, and forestry as well as non-food energy crops [2-5]. Furthermore, biomass is appealing due to it is ubiquitous and readily available worldwide. In addition, it has potential conversion efficiency and the ability to produce and consume on a CO_2-neutral basis [2].

Various biomass sources, such as FT wax [6], soybean [7], and palm oil [8], have been reported to be able to generate biofuel and biodiesel through catalytic hydrocracking process. Aside

* Corresponding Author.
E-mail: wegats@ugm.ac.id (W. Trisunaryanti)
Telp: +62 274 545188

from those sources, *Calophyllum inophyllum* oil (CIO) as a non-edible biomass resource is a potential source of biofuel. The kernels of CIO have very high oil content (75%) which is composed of approximately 71% of unsaturated fatty acids (oleic and linoleic acids) [9]. The appearance of CIO is similar to olive oil, with an aromatic odor and an insipid taste [10]. The conversion of CIO into biodiesel has been carried out via pre-treatment giving the yield of biodiesel from the CIO under the optimized conditions is found to be 89% [11]. Other studies [12,13] found that the characterization test of CIO biodiesel is very close agreement to the diesel oil which is potential to be directly used for diesel engines. Conversion of bio-oil, in this case CIO, can be conducted through hydrocracking which includes hydrogenation and cracking reactions that take place simultaneously [7]. To achieve an optimum conversion of CIO, the catalyst should present in the hydrocracking reaction.

Supported precious metals as well as transition metals have been studied for the hydrocracking reaction [14-17]. However, despite its good catalytic activity, the use of precious metal as a catalyst is considered as cost-ineffective and the utilization of mere low-cost transition metals cannot compete with precious metals catalytic performance. Therefore, optimizing an appropriate catalytic system is required. One of the reported alternatives is by designing heterogeneous catalysts based on the transition metals supported on porous materials [18-20]. It was reported that VI B or VIII B group transition elements, such as W, Mo, Co, and Ni, are active components for hydrogenation catalysis [21]. In addition, designing bimetallic catalysts, such as Co-Mo, is reported to highly efficient for several catalytic performances [22-24]. Moreover, the bimetallic catalyst composed of Co-Mo has a prominent influence on catalytic activity [25].

Considering our previous investigation [26] by employing Ni and/or Mo based catalyst on γ-Al_2O_3 on hydrocracking of CIO that exhibited quite satisfying results, in this study, we employed Co and/or Mo based catalyst on γ-Al_2O_3 support material evaluated in the same reaction. The catalysts were prepared through a simple impregnation method. In addition, the metal loading was set distinct from the previous investigation.

2. Materials and Methods

2.1 Materials

The materials used for the investigation; $Co(NO_3)_2 \cdot 6H_2O$ (purity 99%), $(NH_4)_6Mo_7O_{24} \cdot 4H_2O$) (purity 99%), and γ-Al_2O_3; were purchased from Merck. N_2 gas and H_2 gas were supplied by Samator Ltd., while CIO (density of 0.893 g cm^{-3}; viscosity of 41.0 mPa.s; 31.4% saturated fatty acid; 68.6% unsaturated fatty acid) was originated from Cilacap, Indonesia.

2.2 Catalyst Preparation

The preparation of monometallic and bimetallic catalysts of Co and/or Mo was conducted by using a simple wet impregnation method. The monometallic catalysts of were set to have 10 wt% (marked as a) of metal content denoted as $_aCoO/\gamma$-Al_2O_3 and $_aMoO/\gamma$-Al_2O_3 while bimetallic catalyst was set to have 5 wt% (marked as b) and 10 wt% of each metal content denoted as $_aCoO_aMoO/\gamma$-Al_2O_3 and $_bCoO_bMoO/\gamma$-Al_2O_3. The only difference between monometallic and bimetallic catalysts preparation was the mixing of Co and Mo salt precursors prior to the dispersion on γ-Al_2O_3 support. Salt precursors of Co and/or Mo were firstly dissolved with double-distilled water followed by dispersion on γ-Al_2O_3. The mixtures were stirred at 70 °C for 20 min. Water was then evaporated and the solids were dried in the oven at 100 °C for 24 h. The dried solids were calcined in N_2 gas stream (20 mL.min^{-1}) at 450 °C for 2 h.

2.3 Catalyst Characterization

The crystallinity of the prepared catalysts was analyzed by an X-ray diffractometer (Rigaku SmartLab Miniflex 600) in the 2θ range of 2-80°. The acidity of catalysts by the gravimetric method using NH_3 gas as the basic adsorbate. Metal content(s) of the catalysts were determined by using Atomic Adsorption Spectrophotometer (Perkin Elmer® 5100 PC). Characteristics of the pores were evaluated according to Brunauer-Emmett-Teller (BET) and Barrett-Joyner-Halenda (BJH) theories using a gas sorption analyzer (Quantachrome® NOVA touch). The surface morphologies of the most excellent catalyst were analyzed using a scanning electron microscope (SEM Hitachi SU-3500®).

2.4 Catalyst Test

Catalytic activity and selectivity of the prepared catalysts were evaluated via hydrocracking of the CIO to produce biofuel (Scheme 1 Appendix). A 21.0 cm length semi-batch stainless steel reactor with an inner diameter of 2.80 cm and an outer diameter of 3.10 cm was used. The catalyst-to-feed weight ratio of 1:100 was determined for the hydrocracking process and

placed inside the reactor. The reactor was sealed and streamed by H_2 gas (30 mL.min^{-1}) at 550 °C for 2 h to ensure that there is no O_2 gas involved in the reaction. Three fractions of products which are liquid, gas, and solid have resulted after hydrocracking reaction ended. The aim product (liquid fraction) was condensed and collected in the heart-shaped-flask. It was further analyzed using gas chromatography-mass spectroscopy (GC-MS Shimadzu® QP2010S). The liquid fraction was further classified according to the number of composed carbons which are gasoline fraction (C_6-C_{12}) and diesel fraction (>C_{12}).

3. Results and Discussion

3.1 Catalyst Preparation and Characterization

With the aim to develop an alternative catalyst for the conversion of biomass, the prepared catalysts show the suitability for hydrocracking of CIO. Table 1 shows the results of total metal loading in the catalysts show that the metal(s) were not fully deposited on the catalyst support as the wt% of the total loading is lower than intended to be. This might be happened due to the mass loss during the preparation process. The loading of metal(s) on support material changed its properties. It caused a decrease in surface area and pore volume because the metal particles filled up the pores. The $_aCoO_aMoO/\gamma$-Al_2O_3 catalyst with the highest metal content shows a significant decrease in surface area and pore volume.

The presence of metal on the support material has been reported can increase its acidity as it can provide Lewis acid site which is in accordance with this study [25]. This Lewis acid site is preferable in many chemical reactions including hydrocracking reaction. The acidity of the prepared catalysts is shown in Table 1. Without the impregnation of metal(s), the acidity of γ-Al_2O_3 was 2.08 mmol.g^{-1}. Based on Table 1, the acidity of γ-Al_2O_3 was increased by the presence of metal species. In addition, the total amount of metal loaded will also affect the acidity. A higher total amount of metal will give higher acidity. However, not all prepared catalysts are in line with this theoretical approach. The acidity of $_aCoO_aMoO/\gamma$-Al_2O_3 catalyst which has the highest metal loading was only 5.01 mmol.g^{-1}, lower than $_bCoO_bMoO/\gamma$-Al_2O_3 catalyst which has only 7.35 wt% metal loading. This phenomenon might be occurred due to the big particle metal species generated on $_aCoO_aMoO/\gamma$-Al_2O_3 decreases the active site of the catalyst. Moreover, the generated big particles may also block the pore of γ-Al_2O_3 which also decreases the active sites. This phenomenon is confirmed by surface analysis results.

The adsorption-desorption analysis utilizing N_2 gas molecule with Brunauer-Emmett -Teller (BET) theory allows us to identify the physical properties of the catalyst. In addition, by employing the Barrett-Joyner-Halenda (BJH) method, the pore distribution of the catalyst can be observed. According to the physical sorption analysis shows in Figure 1, all prepared catalyst generated hysteresis loop which indicates the pore sizes are in the range of mesoporous material (identified as type IV adsorption). As shown in Figure 1, the volume of N_2 gas adsorbed is decreased after the impregnation of metals(s). The lowest volume of N_2 gas adsorbed in $_aCoO_aMoO/\gamma$-Al_2O_3 was due to the high metal loading that impregnated on the support. As a result, the volume of N_2 gas adsorbed will be decreased.

There was quite a decrease in specific surface area in $_aCoO_aMoO/\gamma$-Al_2O_3 while there was no significant gap in other catalysts. The more metals loading might cause more aggregates in the metal particles that lead to the inhomogeneous deposition on the support or even might block the pore. In addition, the pore volume and average pore diameter are in accordance with the specific surface area which is decreased with the deposition of metal particles.

Table 1. Physical and chemical properties of the catalyst

Samples	Metal Loading (wt%)			Acidity	S_{BET}	Pore Volume	Average pore
	Co	Mo	Total	(mmol.g^{-1})	(m^2.g^{-1})	(cm^3.g^{-1})	diameter (nm)
γ-Al_2O_3	-	-	-	2.08	127.18	0.21	3.31
$_aCoO/\gamma$-Al_2O_3	6.17	-	6.17	3.89	126.53	0.18	2.90
$_aMoO/\gamma$-Al_2O_3	-	7.18	7.18	4.87	125.77	0.18	2.90
$_aCoO_aMoO/\gamma$-Al_2O_3	6.31	7.31	13.62	5.01	107.67	0.15	2.86
$_bCoO_bMoO/\gamma$-Al_2O_3	3.08	4.27	7.35	5.32	122.84	0.18	2.95

The evaluation of pore radius by BJH method (Figure 2) shows that without experiencing the impregnation process, pure Al_2O_3 has the most homogeneous pore distribution indicated by the high and narrow peak [26]. After metal(s) deposition, the homogeneity of the pore radius is slightly changed while maintaining the radius range. The low homogeneity of pore radius was due to the distinct amount of the loaded metals. In this sense, the more metal(s) loaded will tend to decrease the homogeneity of the pores. With that being said, it is important to control the preparation method to generate more homogeneous metal(s) dispersion which is expected to have better catalytic performance.

The impregnated metal(s) species were characterized using X-ray diffractometer. As shown in Figure 3, the XRD pattern of γ-Al_2O_3 support material indicated by the broad peak at 2θ started around 20° showing its amorphous character. In addition, it was also indicated at 2θ around 45° and 67°. The trend of γ-Al_2O_3 characteristic peaks was observed in all prepared catalyst denoting that the impregnation of metal(s) did not damage the support materials.

In the monometallic catalyst of $_a$CoO/γ-Al_2O_3, the characteristics of cobalt species in the form of oxide were present at 2θ around 27°, 38°, 56°, 59°, and 63° (JCPDS no. 00-002-0770). While in the MoO/γ-Al_2O_3, the molybdenum oxide species were present at 2θ around 37°, 42°, and 60° (JCPDS no. 01-074-4517). On the other hand, in the bimetallic catalysts of $_a$CoO$_a$MoO/γ-Al_2O_3 and $_b$CoO$_b$MoO/γ-Al_2O_3, the new peaks correspond to the Co-Mo-oxide species were detected at the similar 2θ around 18°, 25°, 32°, 37°, 56°, and 59° (JCPDS no. 00-021-0869). This shows that the impregnation of bimetallic CoMo was proceeded generating distinct XRD patterns from a monometallic metal impregnation.

SEM analysis was conducted to see the morphology of the catalysts. Moreover, the effect of impregnation can be observed by the SEM images of γ-Al_2O_3 (Figure 4A) and after impregnation of metals represented by $_a$CoO$_a$MoO/γ-Al_2O_3 catalyst (Figure 4B). Based on the images, the impregnation of metals resulted in a very distinct morphology of the support surface indicating that the metals have successfully deposited on the support material.

3.2 Catalytic Activity

The catalytic performance of the prepared catalysts was evaluated on the hydrocracking of the CIO carried in a fixed-bed reactor. CIO as a bio-oil is a thick-dark green liquid. After it

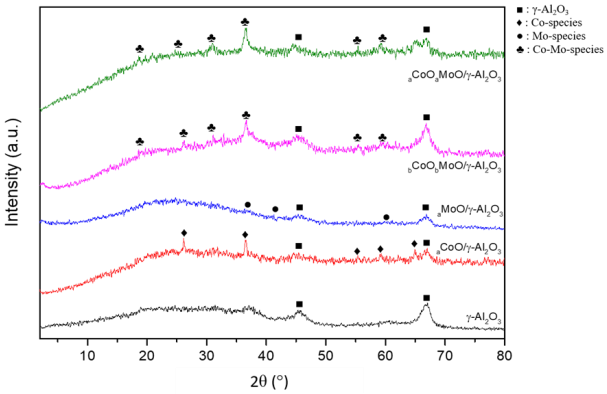

Figure 3. XRD patterns of catalysts

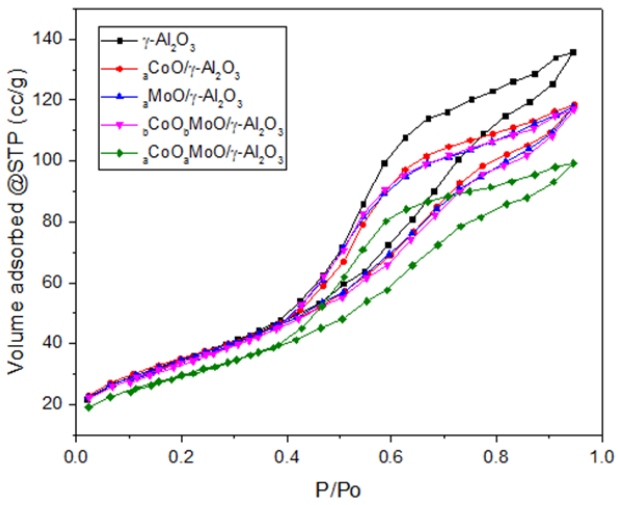

Figure 1. Isotherm adsorption and desorption of the catalysts

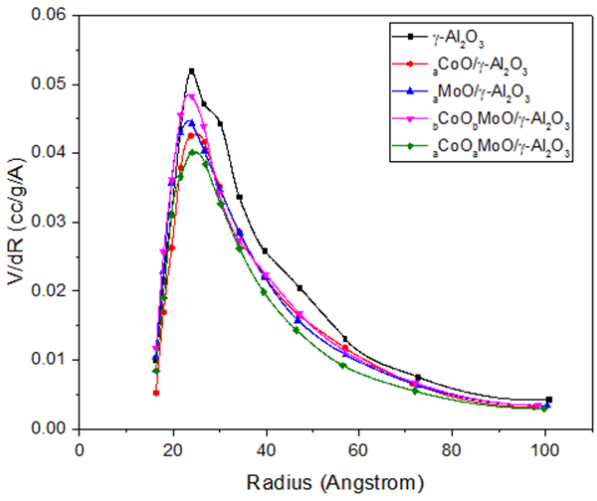

Figure 2. Pore radius distribution of the catalysts

is converted into biofuel by heating and streaming with H_2 gas, it turns into the thinner and lighter green to yellowish liquid. As summarized in Table 2, thermal hydrocracking as well as hydrocracking with pure support material were conducted to have a clearer observation. During the hydrocracking process, three fractions of products (liquid, gas, and coke) were generated. A previous reported investigation [28] stated that thermal hydrocracking prefers to produce gases because the reaction is carried out via the formation of radical ions in high temperature without catalyst generating short carbon chains (mostly gases). On the other hand, the catalytic hydrocracking proceeds through the formation of carbo-cations to produce longer carbon chains (liquids). This is aligned with the present investigation.

Table 2 summarized the product distribution of the hydrocracking of the CIO. As the prepared catalyst is aimed to produce biofuel (liquid), the more liquid fraction produced is desirable. In this case, all prepared catalyst shows mild to good catalytic performance on hydrocracking of CIO. However, $_a$CoO$_a$MoO/γ-Al_2O_3 gave the most satisfying result by producing 65.56 wt% of liquid fraction and selected as the best catalyst in this study with the highest metal content. In this case, the higher liquid product is affected by high metal loading. This is because the presence of catalyst favors to the carbocations formation mechanism that will lead to produce longer carbon chains (liquid). In contrast, proceeding the reaction without a catalyst will favor gas production through the formation of radical ions mechanism that generating a short carbon chain. Moreover, in terms of undesired coke formation, this catalyst also showed the lowest amount of coke with only 0.32 wt%. As shown in Figure 5, there are no significant differences in metal particle size in the SEM images indicating that a very small yield of coke was left on the catalyst. As the formation of coke could deactivate the catalyst and decrease activity, no wonder that $_a$CoO$_a$MoO/γ-Al_2O_3 catalyst with the smallest coke production gave the best catalytic performance on this reaction.

Comparing to our previous report [26] on similar work employing Ni and Mo as catalyst based, the catalytic conversion was quite similar. However, the present study was more superior as the metals were set in a lower total loading (10 wt% for monometallic catalyst; 20

Table 2. The product distribution of hydrocracking of CIO

Catalyst	Metal loading (wt%)	Acidity (mmol.g^{-1})	Hydrocracking product (wt%)		
			Liquid fraction	Coke	Gas fraction
Thermal	-	-	1.69	-	98.31
γ-Al_2O_3	-	2.08	22.31	8.87	68.82
$_a$CoO/γ-Al_2O_3	6.17	3.89	55.48	0.75	44.20
$_a$MoO/γ-Al_2O_3	7.18	4.87	46.08	0.77	53.26
$_a$CoO$_a$MoO/γ-Al_2O_3	13.62	5.01	65.56	0.32	33.67
$_b$CoO$_b$MoO/γ-Al_2O_3	7.35	5.32	60.83	0.66	38.42

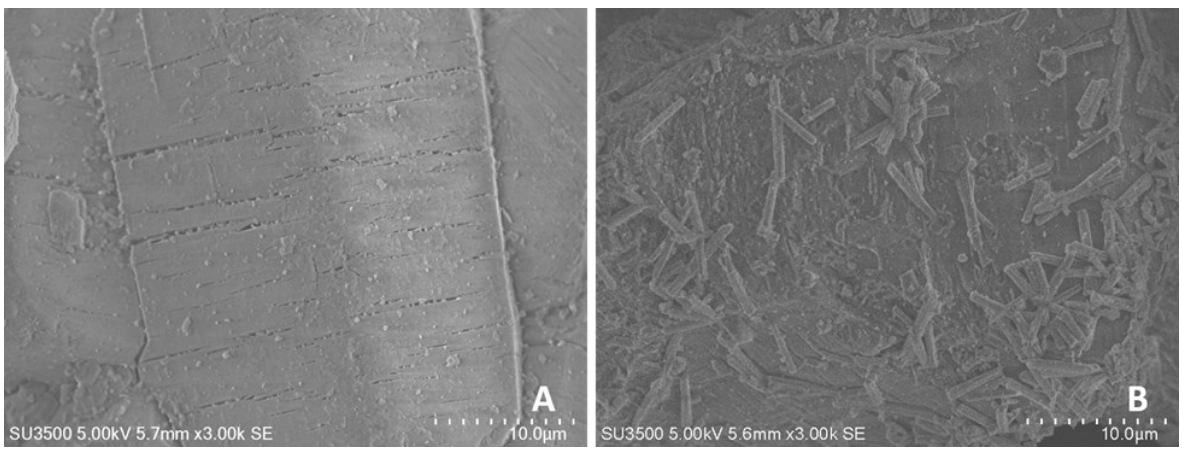

Figure 4. SEM images of (A) γ-Al_2O_3 and (B) $_a$CoO$_a$MoO/γ-Al_2O_3

wt% for bimetallic catalyst) than the previous one (15 wt% for monometallic catalyst; 30 wt% for bimetallic catalyst). Moreover, although in the end the amount of deposited metal on the support was similar, the present study shows that the impregnation process was more successful. In addition, other similar research employing CoMo/γ-Al_2O_3 with higher metal loading gave lower liquid product and selectivity [30].

3.3 The Selectivity of Liquid Product

The generated liquid product was characterized by GC-MS and the compositions were grouped into gasoline fraction (C_6-C_{12}) and diesel fraction (>C_{12}). Based on the previous reports [28,29], the retention time for gasoline was <30 minutes while diesel was >30 minutes. The major product of the hydrocracking reaction is summarized in Table 3. According to Table 3, each catalyst shows different compound compositions. In terms of selectivity, the $_b$CoO$_b$MoO/γ-Al_2O_3 catalyst is likely to have better selectivity toward the liquid product composition with 9.11 wt% gasoline and 7.52 wt% diesel compared to $_a$CoO$_a$MoO/γ-Al_2O_3 catalyst with the highest yield liquid product composed of 8.61 wt% gasoline and 5.01 wt%

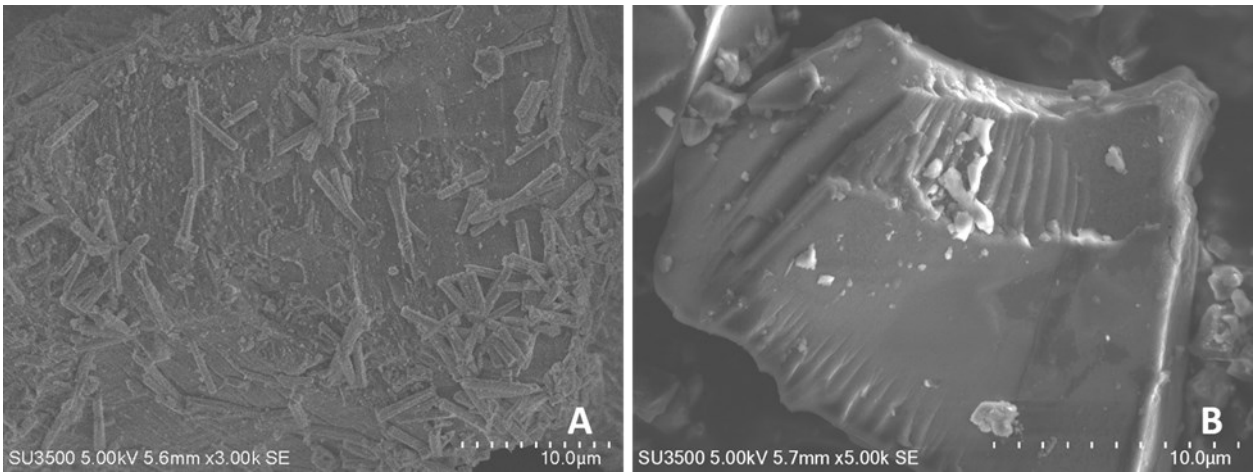

Figure 5. SEM images of $_a$CoO$_a$MoO/γ-Al_2O_3 (A) before hydrocracking and (B) after hydrocracking

Table 3. Major components of the liquid product

Molecular formula	Product percentage (wt%)				
	γ-Al_2O_3	$_a$CoO/γ-Al_2O_3	$_a$MoO/γ-Al_2O_3	$_b$CoO$_b$MoO/ γ-Al_2O_3	$_a$CoO$_a$MoO/ γ-Al_2O_3
C_7H_{16}					0.11
C_8H_{18}			0.19	0.19	0.30
C_9H_{20}		0.43	0.46	0.33	0.46
C_9H_{18}				0.69	0.47
C_9H_{16}		0.41	0.27	0.49	0.24
$C_{10}H_{22}$	0.16		1.13	6.39	5.38
$C_{10}H_{20}$			0.48		1.65
$C_{11}H_{22}$	0.50	1.16	1.34	1.02	
$C_{11}H_{24}$					
$C_{12}H_{26}$	0.69	0.51	2.31		
$C_{12}H_{24}$	0.16	0.98	0.77		
$C_{13}H_{28}$		1.31			
$C_{16}H_{32}$	0.32	0.92	0.35	1.10	0.78
$C_{17}H_{34}$	0.78	2.42	0.59	6.42	4.23
Others	19.70	37.94	47.59	44.20	51.94
Total	22.31	46.08	55.48	60.83	65.56

diesel. Despite its low production of liquid fraction, the product of hydrocracking process employing γ-Al_2O_3 without metal species favor long carbon chains. On the other hand, employing metal(s) impregnated on the support favor to the gasoline fraction.

4. Conclusions

The deposition of metal(s) on γ-Al_2O_3 was successfully conducted through simple wet impregnation. The prepared monometallic catalysts of ${}_aCoO/\gamma$-Al_2O_3 and ${}_aMoO/\gamma$-Al_2O_3, as well as bimetallic catalysts of ${}_aCoO_aMoO/\gamma$-Al_2O_3 and ${}_bCoO_bMoO/\gamma$-Al_2O_3, were characterized and evaluated in the hydrocracking of CIO. Out of the prepared catalysts, ${}_aCoO_aMoO/\gamma$-Al_2O_3 with total metal content, acidity and specific surface area of 13.62 wt%, 5.01 mmol.g^{-1}, and 107.67 m^2.g^{-1}, respectively, showed best catalytic performance by producing 65.56 wt% liquid fraction. This high production of liquid product was due to its high metal content that favors the carbocations formation mechanism that generates longer carbon chains (liquid phase). It was selective to produce 8.61 wt% gasoline and 5.01 wt% diesel.

Acknowledgments

This research was supported by Faculty Mathematics and Natural Sciences Universitas Gadjah Mada under the scheme of Lecturer Research Grant 2020 (Contract number: 56/J01.1.28/PL.06.02/2020).

References

[1] Woo, Y., Cho, S., Kim, J., Kim, B.S. (2016). Optimization-based approach for strategic design and operation of a biomass-to-hydrogen supply chain. *International Journal Hydrogen Energy*, 41, 5405–5418.

[2] Iakovou, E., Karagiannidis, A., Vlachos, D., Toka, A., Malamakis, A. (2010). Waste biomass-to-energy supply chain management: a critical synthesis. *Waste Management,* 30, 1860-1870.

[3] Chambost, V., Stuart, P.R. (2007). Selecting the most appropriate products for the forest biorefinery. *Industrial Biotechnology*, 3, 112-119.

[4] Dui, N., Guzovi, Z., Cosi, B., Stani, Z. (2011). Geographic distribution of economic potential of agricultural and forest biomass residual for energy use: case study Croatia. *Energy*, 36, 2017-2028.

[5] Perego, C., Bosetti, A. (2011). Biomass to fuels: The role of zeolite and mesoporous materials. *Microporous Mesoporous Materials*, 144, 28–39.

[6] Priyanto, U., Suprapto, S., Roesyadi, A., Rosyadi, E., Nurunnabi, M., Hanaoka, T., Miyazawa, T., Sakanishi, K. (2011). Biofuel Production by Hydrocracking of Biomass FT Wax over NiMo/Al_2O_3-SiO_2 Catalyst. *Journal of the Japan Institute of Energy*, 90, 1171-1176.

[7] Zhou, Z., Zhang, W., Sun, D., Chu, L., Jiang, J. (2016). Renewable biofuel production from hydrocracking of soybean biodiesel with a commercial petroleum Ni-W catalyst. *International Journal of Green Energy*, 13, 1185-1192.

[8] Ssrihanun, N., Dujjanutat, P., Muanruksa, P., Kaewkannetra, P. (2020). Biofuels of Green Diesel–Kerosene–Gasoline Production from Palm Oil: Effect of Palladium Cooperated with Second Metal on Hydrocracking Reaction. *Catalysts*, 10:241.

[9] Said, T., Dutot, M., Martin, C., Beaudeux, J. L., Boucher, C., Enee, E., Baudoin, C., Warnet, J-M., Rat, P. (2007). Cytoprotective effect against UV-induced DNA damage and oxidative stress: role of new biological UV filter. *European Journal of Pharmaceutical Sciences*, 30, 203–210.

[10] Ong, C.H., Mahlia, I.M.T., Masjuki, H.H., Norhasyima, R.S. (2011). Comparison of palm oil *Jatrophacurcas* and *Calophyllum inophyllum* for biodiesel. *Renewable Sustainable Energy Review*, 15, 3501-3515.

[11] Venkanna, B.K., Reddy, C.V. (2009) Biodiesel production and optimization from Calophyllum inophyllum Linn oil (honne oil) – a three stage method. *Bioresource Technology*, 100, 5122–5125.

[12] Sahoo, P.K., Das, L.M. (2009). Process optimization for biodiesel production from Jatropha Karanja and Polanga oils. *Fuel*, 88, 1588–1594.

[13] Sahoo, P.K., Das, L.M., Babu, M.K.G., Naik, S.N. (2007). Biodiesel development from high acid value polanga seed oil and performance evaluation in a CI engine. *Fuel.*, 86, 448–454.

[14] Maki-Arvela, P., Rozmyszowicz, B., Lestari, S., Simakova, O., Eranen, K., Salmi, T., Murzin, D.Y. (2011). Catalytic deoxygenation of tall oil fatty acid over palladium supported on mesoporous carbon. *Energy & Fuel*, 25, 2815–2825.

[15] Murata, K., Liu, Y., Inaba, M., Takahara, I. (2010). Production of synthetic diesel by hydrotreatment of jatropha oils using Pt−Re/H-ZSM-5 catalyst. *Energy Fuel*, 24, 2404–2409.

[16] Sotelo-Boyas, R., Liu, Y., Minowa, T. (2011). Renewable diesel production from the hydrotreating of rapeseed oil with zeolitic and

$NiMo/Al_2O_3$ catalysts. *Industrial & Engineering Chemistry*, 50, 2791–2799.

[17] Yang, R., Du, X., Zhang, X., Xin, H., Zhou, K., Li, D., Hu, C. (2019). Transformation of Jatropha Oil into High-Quality Biofuel over Ni-W Bimetallic Catalysts. *ACS Omega*, 4, 10580–10592.

[18] Albayanti, T.M., Doyle, A.M. (2014). SBA-15 supported bimetallic catalysts for enhancement isomers production during n-heptane decomposition. *International Journal of Chemical Reactor Engineering*, 12, 345–354.

[19] Grilc, M., Likozar, B., Levec, J. (2014). Hydrodeoxygenation and hydrocracking using different catalyst. *Applied Catalysis B: Environmental,* 150–151, 275–287.

[20] Rianto, L. B., Amalia, S., Khalifah, S.N. (2012). Effect of metal impregnation on natural zeolite towards zeolite surface area. *Alchemy,* 2, 58–67.

[21] Li, X., Qiao, K., Subhan, F., Xing, W., Liu, X., Yan, Z. (2015). Preparation and hydrodesulfurization properties of cobalt–molybdenum–phosphorous catalysts for removal of dibenzothiophene. *Applied Petrochemical Research*, 5, 405–411.

[22] Li, G., Yue, L., Fan, R., Liu, D., Li, X. (2017) Synthesis of a Co-Mo sulfide catalyst with a hollow structure for highly efficient hydrodesulfurization of dibenzothiophene. *Catalysis Science & Technology*, 7, 5505-5509.

[23] Yamada, S., Qian, W., Ishihara, A., Ichinoseki, M., Kabe, T. (2001). Methods of Activating Catalysts for Hydrodesulfurization of Light Gas Oil (Part 1) Catalytic Activity of $CoMo/Al_2O_3$ Catalyst Presulfided with Polysulfides for Hydrodesulfurization of Dibenzothiophene. *Sekiyu Gakkaishi*, 44, 217-224.

[24] Pongsendana, M., Trisunaryanti, W., Artanti, F.W., Falah, I.I., Sutarno, S. (2017), Hydrocracking of waste lubricant into gasoline fraction over CoMo catalyst supported on mesoporous carbon from bovine bone gelatin. *Korean Journal of Chemical Engineering*, 34, 2591-2596.

[25] Al-Zeghayer, Y., Sunderland, P., Al-Masry, W., Al-Mubaddel, F., Ibrahim, A., Bhartiya, B.K., Jibril, B. (2005). Activity of $CoMo/\gamma$-Al_2O_3 as a catalyst in hydrodesulfurization: effects of Co/Mo ratio and drying condition. *Applied Catalysis A: General*, 282, 163–171.

[26] Trisunaryanti, W., Kartika, I.A., Mukti, R.R., Hartati, H., Triyono, T., Widyawati, R., Suarsih, E. (2019), Preparation of Ni- and Mo-based catalysts supported on γ-Al_2O_3 for hydrocracking for *Calophyllum inophyllum* oil, *Biofuels.*, doi: 10.1080/17597269.2019.1669871

[27] Trisunaryanti, W., Suarsih, E., Falah, I.I., Triyono, T. (2019) Well-dispersed nickel nanoparticles on the external and internal surface of SBA-15 for hydrocracking of pyrolyzed a-cellulose. *RSC Advances*, 9, 1230–1237.

[28] Khowatimy, F.A., Priastomo, Y., Febriyanti, E., Riyantoko, H., Trisunaryanti, W. (2014). Study of waste lubricant hydrocracking into fuel fraction over the combination of Y-zeolite and ZnO catalyst, *Procedia Environmental Sciences,* 20, 225–234.

[29] Wijaya, K., Syoufian, A., Ariantika, S.D. (2014). Hydrocracking of used cooking oil into biofuel catalyzed by nickel-bentonite. *Asian Journal of Chemistry*, 26, 3785–3789.

[30] Rasyid, R., Prihartantyo, A., Mahfud, Roesyadi, A. (2015). Hydrocracking of Nyamplung Oil (*Calophyllum inophyllum oil*) Using $CoMO/\gamma$-Al_2O_3 and $CoMo/SiO_2$ Catalysts. *Modern Applied Sciences,* 9, 43-47.

Appendix. Experimental Reactor Scheme

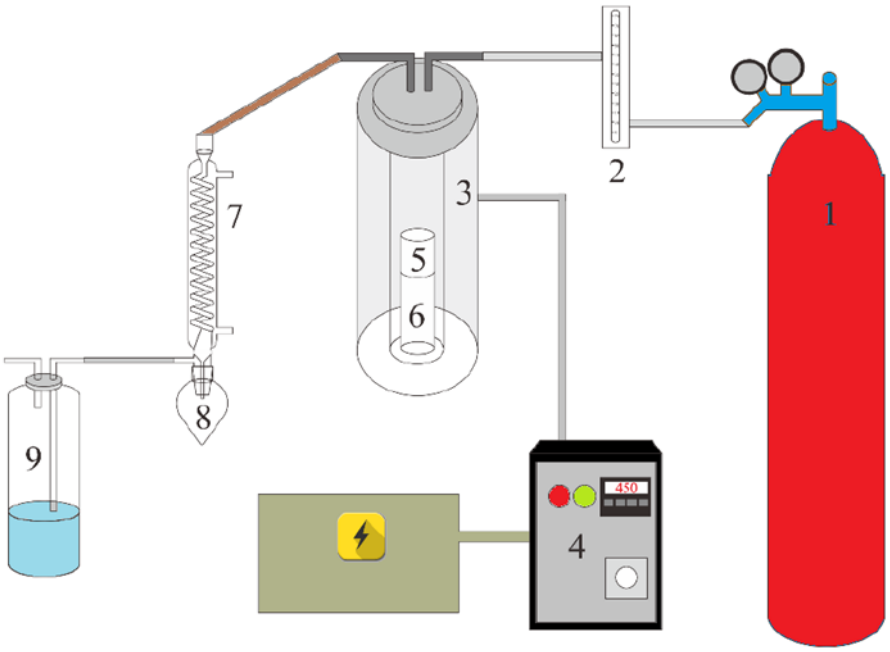

Notes:
1. Hydrogen gas
2. Gas flow meter
3. Furnace
4. Thermocouple
5. Catalyst vessel
6. Feed vessel
7. Condenser
8. Heart shaped flask
9. Gas trapper

Calculation on product distribution:

$$\text{Liquid Fraction (\%)} = \frac{w_{h1} - w_{h0}}{w_f - (w_{r1} - w_{r0})} \; x \; 100\ \%$$

$$\text{Coke (\%)} = \frac{w_{c1} - w_{c0}}{w_f - (w_{r1} - w_{r0})} \; x \; 100\ \%$$

Gas Fraction (%) = 100 % - liquid fraction - coke

Where, w_f is weight of feed (pyrolyzed α-cellulose), w_{h0} is weight of empty heart shaped flask, w_{h1} is weight of heart shaped flask after hydrocracking, w_{c0} is weight of catalyst before hydrocracking, w_{c1} is weight of catalyst after hydrocracking, w_{r0} is weight of empty reactor, and w_{r1} is weight of reactor after hydrocracking.